ELSEVIER

International Journal of Mass Spectrometry 189 (1999) 133–146

International Journal of Mass Spectrometry

Influence of the primary ion beam parameters (nature, energy, and angle) on the kinetic energy distribution of molecular fragments sputtered from poly(ethylene terephthalate) by kiloelectron volt ions

A. Delcorte[a,*], X. Vanden Eynde[a], P. Bertrand[a], D.F. Reich[b]

[a]*Unité de Physico-Chimie et de Physique des Matériaux, Université Catholique de Louvain, 1 pl. Croix du Sud, B-1348 Louvain-la-Neuve, Belgium*

[b]*Physical Electronics, 575 Chesapeake Drive, Redwood City, CA 94093, USA*

Received 2 February 1999; accepted 12 April 1999

Abstract

Thin films of poly(ethylene terephthalate) (PET) cast on silicon were bombarded by 2–22 keV In^+ ions and 12 keV Ga^+ ions and the positive secondary ions were mass and energy analysed by means of a time-of-flight secondary ion mass spectrometer. Since the secondary ion intensities are seen to be dependent on the primary beam parameters, the purpose of this work was to check if these parameters (mass, primary energy, and incidence angle) also influence the kinetic energy distributions of the sputtered molecular fragment ions. This is done in order to gain a better understanding of the molecular ion emission from polymer targets. In general, the shape of the kinetic energy distribution of PET fragment ions is found to be almost independent upon the primary ion nature and energy, as witnessed by the similar spectra observed with 12 keV Ga^+ and 7–22 keV In^+ primaries. This confirms previous studies which indicated that the main parameters governing secondary ion kinetic energies in this energy range were the secondary ion nature and the chemical structure of the organic and polymer targets. Nevertheless, the energy spectra of the fingerprint fragment ions obtained at 2 keV with an impact angle of 65° with respect to the surface normal are broader than those observed for higher energy and lower angle of incidence (~40°). In comparison with the latter, they exhibit an additional contribution centered around 5–6 eV, i.e. in the high energy tail of the distributions. The integrated intensity of this contribution increases with the fragment size, up to 7% and 15% of the total ion intensity for $C_7H_4O^+$ and $C_{17}H_{12}O_5^+$, respectively. The results are discussed in terms of collision cascade propagation in the surface region of the target, by comparing the experimental observations to simulations conducted with the TRIM code. TRIM calculations suggest that the variation of the impact angle is the predominant factor influencing the atom displacements in the first 25 Å below the surface. In the {2 keV, 65°} configuration, the energy transferred to recoils in this region is similar, but the number of interacting atoms is more than two times greater than for the other tested combinations of energy and angle, suggesting an increased probability of collective processes for molecular ion emission. (Int J Mass Spectrom 189 (1999) 133–146) © 1999 Elsevier Science B.V.

Keywords: Secondary ion mass spectrometry; Sputtering; Ion emission; Kinetic energy; Poly(ethylene terephthalate); TRIM

* Corresponding author. E-mail: delcorte@chem.psu.edu

PII S1387-3806(99)00063-9

1. Introduction

Static secondary ion mass spectrometry (SIMS) has been proven very powerful and is now routinely used for the analysis of organic compounds [1], as witnessed by the growing number of reference spectra in the databases [2]. In contrast, the mechanisms by which large molecular ions may be ejected or desorbed are far from being fully understood. In previous papers, we used the kinetic energy distributions (KED) of these organic ions as a means to improve our knowledge of the fundamental processes in molecular secondary ion mass spectrometry (SIMS). Among them, the following mechanisms have been identified and explained: the emission of low-energy, precursor-like species [3,4], of faster and strongly dehydrogenated ions [5], of rather energetic cationised oligomers and molecules [6], as well as the metastable decay of excited ejecta [7,8]. Our phenomenological model based on the concept of internal energy-dependent fragmentation of excited species accounted for the periodic variation of the hydrocarbon ion kinetic energy [9]. On the other hand, it was shown that a collective collision process is the more appropriate to fit the observed kinetic energies in the case of large parent-like ions [6]. Finally, the observed metastable decay processes could be interpreted with the formalism of the unimolecular reaction theory [10].

In this article, we investigate the effects of the primary beam nature, energy, and incidence angle on the KED of molecular fragments sputtered from poly(ethylene terephthalate) (PET). This work is part of a study devoted to the comparison of the secondary ion (SI) characteristics for different bombardment conditions and polymer samples. The effect of these bombardment conditions on the absolute and relative SI yields will be discussed at length in [11] for poly(styrene), poly(methyl methacrylate) and PET samples. Preliminary results have been presented at the 11th SIMS workshop [12].

Although the emission of molecular ions remains poorly understood, the effects of the primary beam parameters on the yields and KEDs of atomic ions have been investigated in depth. For atomic secondary ions, the increase of the sputtering yield with increasing primary ion energy in the keV range and with increasing incidence angle are well established from the experimental [13,14] and theoretical viewpoints [15]. Although not predicted by the linear collision cascade theory [3,15], the dependence of the KED of sputtered atoms on the primary beam parameters has been observed in the case of light primary ions (H^+, D^+) [16], but also for heavier primaries such as Ar^+ [17] and even Xe^+ [18]. Empirical evidence as well as theoretical calculations [19,20] indicate that the distributions become steeper with decreasing primary ion energy in the keV ion range. On the other hand, the influence of the incidence angle on the KED has been predicted by computer simulation. For nickel bombarded by 1 keV argon, the maximum of the KED shifts to a lower energy, and the high energy tail becomes steeper when the incidence angle varies from 75° to 0° [21]. This effect has been explained by the increased fraction of atoms sputtered by an energetic, single knock-on process at oblique incidence.

Few experimental data exist for molecular ions sputtered from organic overlayers. Standing et al. (reported in [22]), as well as Benninghoven [23], demonstrated the increase of the parent-like ion yields with increasing the primary ion energy, in the case of alanine bombarded with various primary ions ($1 \leq E \leq 16$ keV) [22], and of leucine under Ar^+ bombardment ($1 \leq E \leq 5$ keV) [23], respectively. Benninghoven [23] noted the parallel increase of the damages in the layer. For polymeric targets bombarded by xenon ($1 \leq E \leq 4$ keV), Briggs and Hearn indicated that the increase of the primary beam energy was accompanied by the increase of the total ion yield in some cases, but also by the relative increase of the high mass cluster intensities [24]. This decrease of fragmentation with increasing primary beam energy has been confirmed by Winger, Hand, and Cooks for organic salts cast on metal supports and sputtered by Ar^+ primaries ($1 \leq E \leq 5$ keV) [25]. Nevertheless, it is not always clear from the literature whether energy and angle could be changed independently in the above-mentioned experiments. In the study of Langmuir-Blodgett monolayers of acids and amines, Galéra, Blais, and Bolbach also showed that the

disappearance cross section σ of the $(M–H)^-$ ions (determined from $I = I^O \exp(-\sigma Jt)$; I being the SIMS intensity and J the primary ion flux), increases with increasing primary beam energy ($1 \leq E \leq 7$ keV) and decreasing primary beam-target angle [26]. In addition, they reported a linear relationship between σ and the energy dissipated by the primary ions *in the organic layer*, which was against their previous hypothesis concerning the predominant substrate effect and the collision cascade induced emission [27]. Instead, they proposed an explanation of the ejection of parent ions based on the formation of a vibrationally excited region. Galéra et al. studied the fragmentation of the parent ions sputtered from similar films, too [28]. They evidenced the decrease of the fragmentation with increasing primary Cs^+ ion energy for gold but not for silver substrates and proposed an interpretation based on the difference of binding energies for the two substrates. Concerning the effect of the incidence angle, Martin, Costello, and Biemann [29] as well as Szymczak and Wittmaack [30] demonstrated the increase of the molecular ion sputtering yield with increasing incidence angle, as was the case for atomic ions. Recently, Kudo and co-workers used a similar apparatus as ours to investigate the effects of the primary beam energy and angle on the yield of secondary ions sputtered from cadmium arachidate monolayers on silver [31,32], alkanethiols on gold [32], and thin fluorolubricant layers [33]. For all these systems, they showed the relative decrease of the substrate ion intensity with increasing incidence angle, indicating the reduction of the sampling depth at glancing incidence.

On the other hand, molecular dynamics (MD) simulation studies have been conducted to test these effects in the case of organic molecule sputtering. For benzene adsorbed on nickel, Garrison found that the fragment and molecular species yields increase in parallel with increasing primary ion energy (100 eV $\leq E \leq$ 1500 eV) [34]. With very low primary energies (10 eV $\leq E \leq$ 100 eV), the same trend was demonstrated for biphenyl molecules adsorbed on copper [35]. Concerning the effect of the primary beam angle, this group has shown that the total ion yield as well as the fragmented molecule fraction increases when changing from normal to off-normal incidence (45°) for pentylidyne adsorbed on platinum [36].

2. Materials and methods

2.1. Samples

The PET was dissolved in hexafluoro-4-isopropanol. The samples were prepared as thin films cast on silicon substrates (1 cm^2), by depositing a droplet of the solution on the supports. Prior to deposition, the substrates were rinsed in water of high-performance liquid chromotography (HPLC) grade from a milli-*Q* system (Millipore), isopropanol and hexane. The low concentration of the solutions allowed us to deposit very thin polymer layers, ensuring a good electric contact between the top surface and the sample holder. In this way, charging effects could be avoided. In the same time, care was taken to eliminate the influence of the silicon substrate on the secondary ion yields, by using samples for which the silicon ion intensity was sufficiently weak. This procedure has been fully described in [10]. All the energy measurements were conducted with samples respecting these requirements. Such samples could be reproducibly built up from properly dosed PET solutions.

2.2. Time-of-flight SIMS setup

The secondary ion mass analyses and the KED measurements were performed in a PHI-EVANS time-of-flight (TOF) SIMS (TRIFT 1) using (5 kHz) pulsed Ga^+ and In^+ beams (~500 pA dc) [37]. The angle between the primary ion source and the spectrometer axis (perpendicular to the surface) was 35°. The primary beam conditions (nature, energy, and calculated impact angle) are listed in Table 1. In our system, the different primary ion energies result in different beam impact angles due to the high electric field in the acceleration section of the spectrometer. After emission, the secondary ions were accelerated between the sample surface (nominal voltage: +3000 V) and the grounded extractor that forms part of the

Table 1
Primary beam conditions (nature, impact energy and angle)

Primary ions	Impact energy (keV)	Impact angle (deg)
Ga^+	12	39.9
In^+	2	65.1
In^+	7	43.3
In^+	12	39.9
In^+	17	38.5
In^+	22	37.7

immersion lens. They were then focused by the immersion lens and transported via a transfer lens, and then deflected 270° by three hemispherical electrostatic analysers (ESA) before reaching the detector (fast dual microchannel plate). For the comparison of absolute yields, all the TOF SIMS spectra were obtained with 1.67×10^8 primary ions, which corresponds to a fluence of 10^{12} ions/cm^2 for the 130×130 μm^2 area sampled in the nominal analysis conditions {12 keV; 39.9°}.

2.3. KED measurements

To obtain the energy spectra, a $+(3000 - \Delta)$ V potential was applied to the sample. At the crossover following the first ESA, where the energy dispersion is maximum, the secondary ions were energy selected by a slit of fixed width (100 μm corresponding to a passband of 1.5 eV). The acquisition of mass spectra for different sample voltages (different Δ) allowed us to collect the signal corresponding to different energy windows of the KED, a 1 V increase of the sample potential corresponding to a 1 eV decrease in the KED. To improve the measured intensities in these KEDs, the secondary ions were postaccelerated by 10 keV before striking the detector. In order to avoid polymer degradation [38] and surface charging during the experiment, the stability of the PET characteristic $C_6H_4CO^+$ ion intensity was confirmed up to a larger primary ion fluence than that needed for one set of measurements on the same area. At least two sets of measurements were conducted on different sample areas for each KED. Between successive sets of measurements, the energy slit was slightly shifted by a distance corresponding to ~0.5 eV. By this means, the second data set covered the intermediate energy windows that were not available from the first data set. In order to combine the two sets of measurements, the zero of the energy scale ($e\ V_0$) for each set was extrapolated from the intersection V_0 between the tangent to the increasing part of the KED of atomic ions and the voltage axis. The initial kinetic energy E_k of the secondary ions was thus obtained using $E_k = e(V_0 - 3000 + \Delta)$. Because unimolecular decomposition reactions in the linear part of the spectrometer can give rise to negative values of E_k [7,8], this quantity will preferably be called "apparent kinetic energy" in the following.

2.4. TRIM calculations

In this study, a Monte Carlo code based on the binary collision model (TRIM [39]) has been used to simulate the penetration and scattering of indium ions in PET. Preliminary results have been obtained with TRIM95 and they were confirmed by SRIM [40]. 5000 trajectories were fully calculated for each set of experimental conditions listed in Table 1. The parameters related to the PET were found in the compound library of the software. The size of the cell was chosen in order to include the whole ion and cascade atom trajectories for each set of bombardment conditions (200 Å $\leq$ thickness $\leq$ 700 Å).

3. Results

3.1. Secondary ion yields and mass spectra

Fig. 1 shows the positive mass spectra of PET obtained with 2, 7, and 22 keV primary indium ions (number of primary ions per spectrum = 1.67×10^8). The most characteristic secondary ions are: $C_6H_4^+$ (m/z = 76), $C_6H_4CO^+$ (m/z = 104), $C_4H_6(COOH)CO^+$ (m/z = 149), and the deprotonated and protonated monomer (m/z = 191,193) [2,41]. Fragments larger than the monomer, including dimers and trimers are also detected: m/z = M + 104; M + 149; $2M$ + 1; $3M$ + 1, where M is the

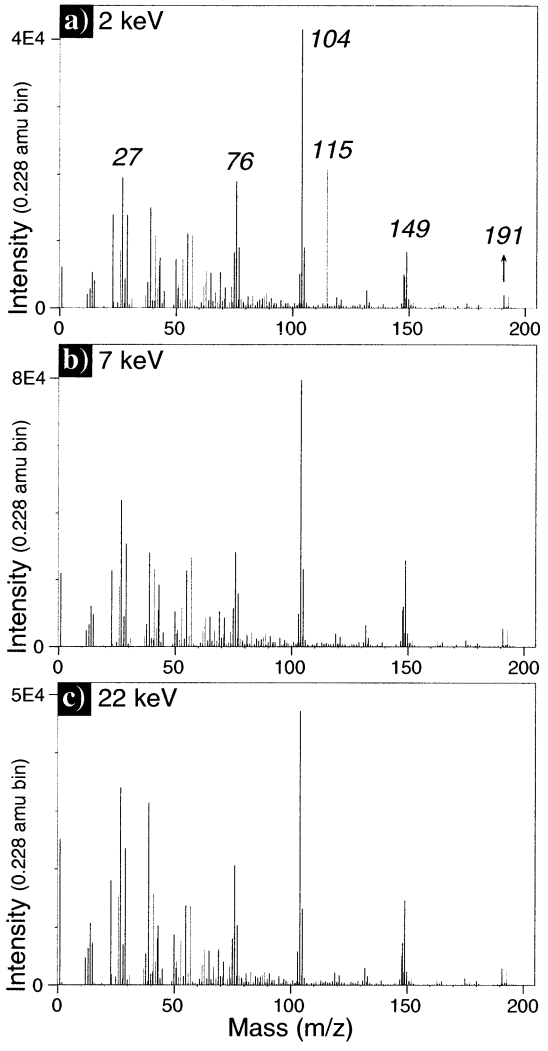

Fig. 1. Positive mass spectra of PET obtained under In^+ bombardment with different primary beam energies and impact angles. (a) 2 keV; 65°; (b) 7 keV; 43.3°; (c) 22 keV; 37.7°.

mass of the monomer (m/z = 192). The predominant hydrocarbon peaks at lower masses ($C_2H_3^+$, $C_2H_5^+$, $C_3H_3^+$, $C_3H_5^+$, etc.) correspond to the fragmentation of the ethylene and phenyl ring of PET, enhanced by the presence of oxygen atoms incorporated in the backbone. The small sodium peak (m/z = 23) denotes a weak contamination of the sample surface. The intense indium peak at m/z = 115 in Fig. 1(a) is due to backscattered primary ions [11], as confirmed by TRIM calculations. The high intensity of backscattered ions can be explained by the very oblique incidence of the beam at the impact point for these analysis conditions.

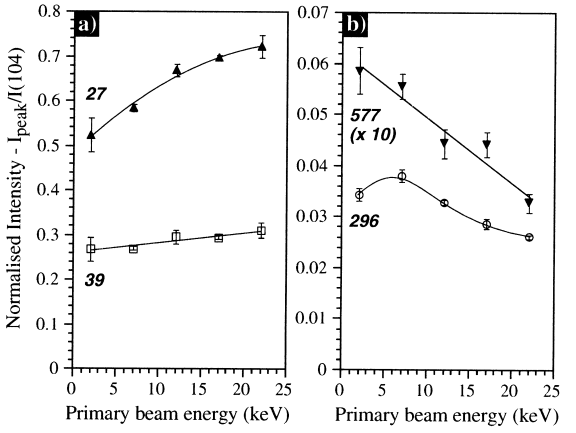

Fig. 2. Relative intensity variation of several characteristic ions of PET. The peak intensities are normalised by the absolute intensity of $C_6H_4CO^+$ (m/z = 104). (a) Small fragment ions; (b) large molecular ions.

As mentioned in Sec. 1, the effect of the primary ion energy on the secondary ion yields will be investigated in detail in [11]. Briefly, it is obvious from Fig. 1 that the absolute intensities are significantly modified when going from 2 to 22 keV impact energy: in general, the peak intensities increase until a maximum corresponding to a primary beam energy of 7 keV and decrease afterwards. Between 2 and 7 keV, the total spectrum intensity increases by a factor of 2. If the parallel decrease of the incidence angle in our measurement could be omitted, the increase of the yields in this region is in agreement with the energy induced variations reported in the literature [22–24]. It is interesting to note that, in our experimental conditions, the SI yields decrease between 7 and 22 keV, which can neither be correlated to the nuclear nor to the electronic stopping power.

On the other hand, the variation of the relative intensities provides some indications concerning the extent of fragmentation of the polymer when the excitation energy increases. The evolution of selected peak intensities, divided by the intensity of $C_6H_4CO^+$ (m/z = 104), are reported in Fig. 2. With increasing primary beam energy, the relative intensity of the

small hydrocarbon peaks ($C_2H_3^+$, $C_3H_3^+$) increases [Fig. 2(a)], although it decreases for large molecular ions including trimers ($m/z = M + 104$, $3M + 1$) [Fig. 2(b)]. This shows that the fragmentation is favoured with higher beam energies for PET bombarded by indium primary ions, in contrast to previous observations with different samples and sputtering conditions [22–25]. To explain this different behaviour, one could argue that the predominant parameter influencing the intensities is the impact angle, which varies significantly with decreasing beam energy between 22 and 2 keV (from 37.7° to 65.1°). However, the shape of the variation remains the same if one excludes the 2 keV measurement, which in turn reduces drastically the impact angle variation (from 37.7° to 43.3°). In this context, a major influence of the incidence angle on the observed intensities can be excluded.

Concerning the influence of the primary beam nature on the polymer fragmentation, it is interesting to compare the spectra of Fig. 1 with the positive spectrum of a similar sample obtained in the Ga^+ {12 keV, 39.9°} bombardment conditions [see [42], Fig. 1(a)]. Whatever the beam energy, the use of indium instead of gallium increases the relative intensity of high-mass clusters (e.g. $m/z = 104$) at the expense of low-mass fragments (e.g. $m/z = 27$). This is consistent with the observation of Briggs and Hearn who found a similar decrease in the extent of fragmentation with increasing primary ion mass [24]. The PET spectra obtained with 8 keV, Cs^+ primaries in a similar TOF SIMS confirm this trend [41].

3.2. Kinetic energy distributions

To gain more information concerning the emission mechanisms, KED measurements were performed with 2, 7, 12, and 22 keV indium and with 12 keV gallium primary ions. Since the intensity of atomic ions sputtered from the PET sample and from the silicon substrate are too weak to measure their KED satisfactorily, the sodium contamination peak will be used as an example. The KED of Na^+ is displayed in Fig. 3 for the 2, 7, and 22 keV bombardment conditions (see Table 1), which means that the step between

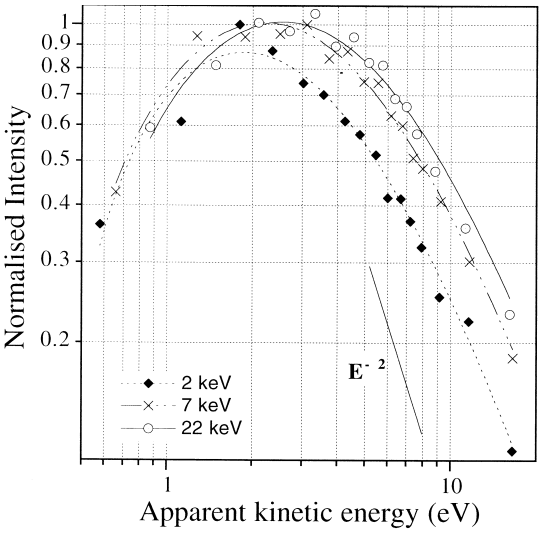

Fig. 3. Kinetic energy distributions of Na^+ sputtered from PET samples bombarded by 2, 7, and 22 keV In^+ primary ions. The lines correspond to the Sigmund-Thompson fit [$Y \sim E/(E + E_b)^3$].

the chosen energies is close to a factor of 3. Although Sigmund's linear collision cascade theory does not take ionisation processes into account, the experimental data were fitted by a Sigmund-Thompson law for comparison purpose. The energy spectra, with a high energy decrease tending to E^{-2}, indicate that the emission of Na^+ is collisional. With decreasing primary beam energy, the width of the distribution decreases (8.4 eV at 22 keV, 7.2 eV at 7 keV, and 4.8 eV at 2 keV) and the maximum shifts to a lower energy (from 2.5 to 1.7 eV). This reduction is reflected by the apparent "binding energy" values deduced from the Sigmund-Thompson fit (4.3 eV at 22 keV, 3.7 eV at 7 keV, and 3.0 eV at 2 keV). Again, the important variation observed between the 2 and 7 keV bombardment conditions is consistent with the literature assuming that the influence of the beam energy [16–20] prevails over the angular effect [21].

Before moving to the case of molecular ions, it is worth remembering the intense indium peak at $m/z = 115$ in the 2 keV mass spectrum. The energy distribution of indium is shown in Fig. 4. It peaks at 3.4 eV, with a full width at half maximum (FWHM) of 5.5 eV, and possess a high energy tail extending beyond 10 eV. This predominance of low-energy backscat-

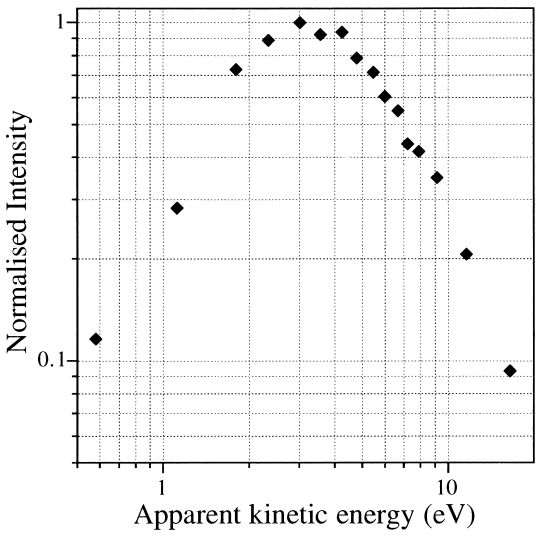

Fig. 4. Kinetic energy spectrum of In^+ backscattered from PET samples bombarded by 2 keV primary ions.

tered ions is well predicted by TRIM calculations (Sec. 3.3). In addition, the energy spectrum of indium ions allows us to check the energy calibration, since backscattered ions having an energy deficit with respect to the energy provided by the acceleration section of the spectrometer are not expected.

The KED of molecular ions sputtered from organic and polymer targets is narrower than that of atomic ions [3,4,7,43,44]. In particular, it has been shown in our previous papers that large characteristic ions are emitted with a low kinetic energy, reflecting a soft emission process, whereas fragmented molecular ions exhibit a higher mean kinetic energy, indicating a more violent ejection mechanism [3–5,7,9]. This has also been verified for PET secondary ions [4]. In Fig. 5, we report the energy spectra of several intense molecular ions observed in the mass spectrum of PET (Fig. 1). As expected, the high energy tail of these distributions is very steep and the measured intensity becomes negligible beyond 10 eV, especially for large characteristic ions (m/z = 76, 104, 296). As the ion size decreases, the energy spectrum broadens gradually (size effect [3]). This is obvious when comparing the KED of $C_2H_3^+$ (m/z = 27) to that of larger molecular ions ($C_6H_4^+$, m/z = 76; $C_6H_4CO^+$, m/z = 104).

Fig. 5(a) and (b) compare the KEDs of $C_2H_3^+$ (m/z = 27) and $C_6H_4CO^+$ (m/z = 104) obtained with 12 keV Ga^+ and In^+ primary ions. The similarity of the measured distributions is striking, especially for $C_6H_4CO^+$.

The KEDs obtained with different primary beam energies are shown in Fig. 5(c)–(f) (In^+ primary ions). Again, the distributions are very similar for 7, 12, and 22 keV, i.e. where the angular variation is weak. The small differences between these measurements are within the experimental error. However, the shape of the distributions obtained with 2 keV and 65° incidence looks different, especially for large characteristic ions. With these analysis conditions, one may note a relative augmentation of the “high energy” fraction (beyond 5 eV). In addition, this fraction increases proportionally to the size of the considered ions. To get a quantitative insight into this phenomenon, the KEDs obtained with 7, 12, and 22 keV have been fitted with a modified Gaussian function, and the additional function needed to account for the high energy part of the 2 keV distributions has been determined. This “decomposition” of the 2 keV KEDs into a low-energy and a high-energy contribution is exemplified in Fig. 5(e) for $C_6H_4CO^+$. After integration of these two curves, one obtains the intensity corresponding to the low-energy (I_{LE}) and to the high-energy (I_{HE}) contributions. The relative fraction corresponding to the high-energy contribution, $I_{HE}/(I_{LE} + I_{HE})$, is shown in Fig. 6 as a function of the secondary ion mass. It increases regularly up to 15% for ion at $m/z = M + 104$.

It has been mentioned in Sec. 3.1 that PET dimers and trimers constitute significant peaks in the positive mass spectrum. The KED of these high mass ions, poorly resolved due to the low intensity, is narrow and very similar to that of lower mass ions ($C_6H_4CO^+$, monomer) (Fig. 7). Despite the poorer counting statistics, Fig. 7 indicates that the FWHM of the distributions does not increase with increasing ion size (trimer as compared to dimer), in contrast with the case of silver-cationised poly(styrene) oligomers [6]. For these large dimer and trimer ions, the weak absolute intensity sampled by the energy slit did not allow us to record the KEDs with the signal-to-noise

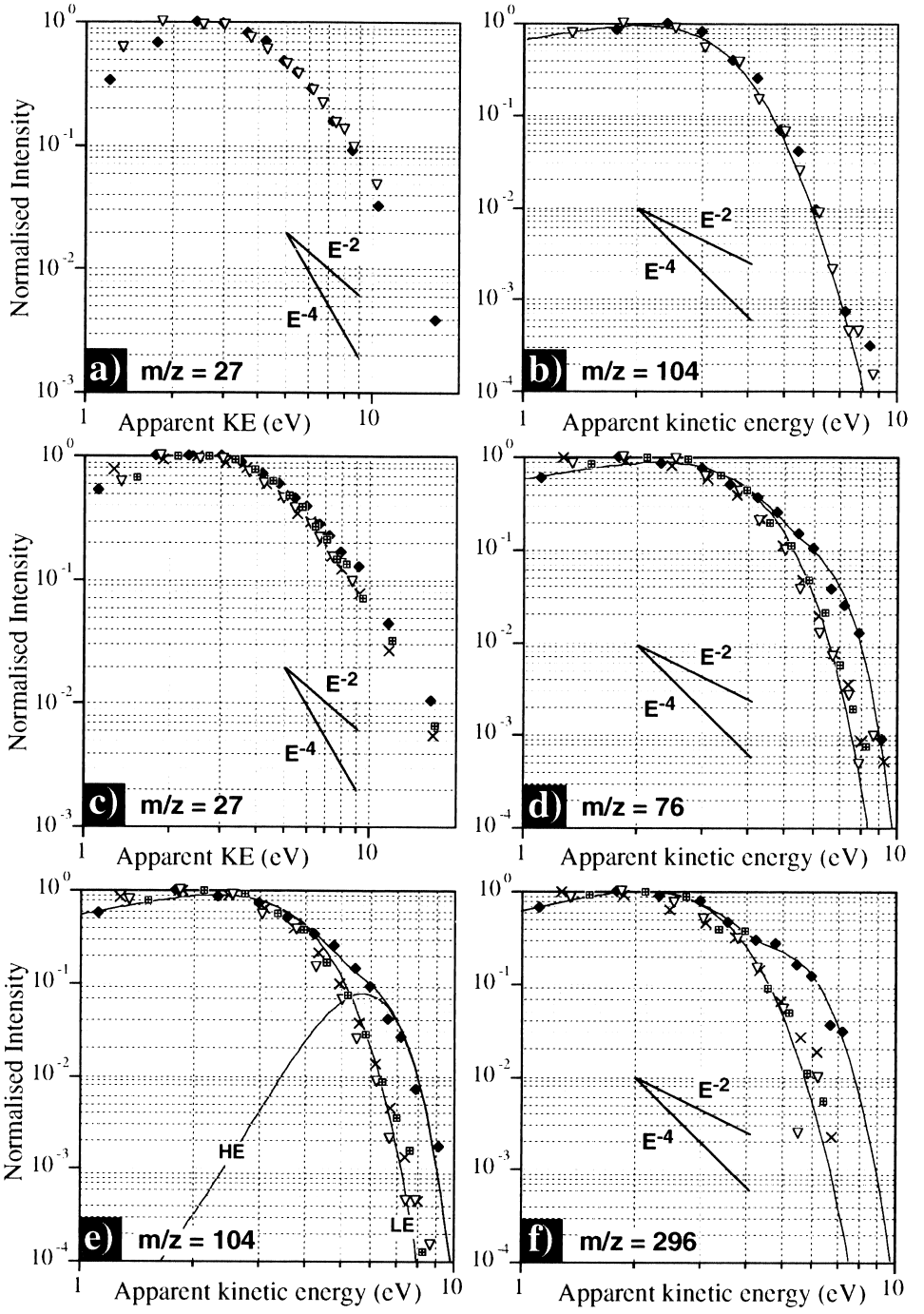

Fig. 5. Kinetic energy distributions of characteristic molecular ions sputtered from PET samples bombarded by 12 keV Ga^+ and 2–22 keV In^+ primary ions. (a) $C_2H_3^+$ for 12 keV Ga^+ (closed circle) and In^+ (inverted open triangle) bombardment; (b) $C_6H_4CO^+$ for 12 keV Ga^+ (closed circle) and In^+ (inverted open triangle) bombardment; (c) $C_2H_3^+$ for 2 (closed circle), 7 (crosses), 12 (inverted open triangle), and 22 keV (plus signs inside squares) In^+ bombardment; (d) ibidem for $C_4H_6^+$; (e) ibidem for $C_4H_6CO^+$; (f) ibidem for the peak at $m/z = M + 104$. See the text for the detail of the curve fittings.

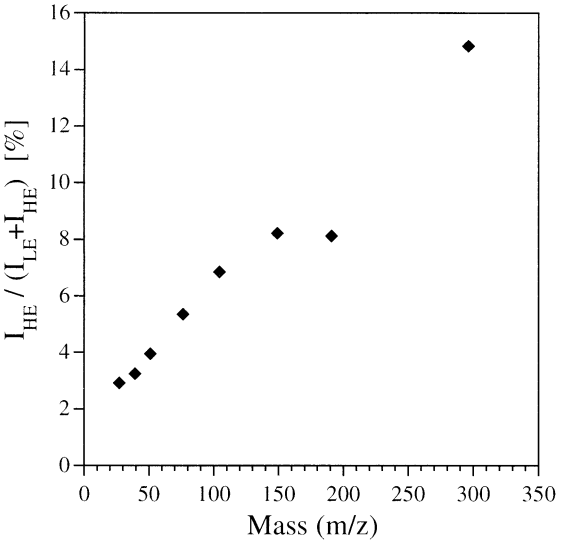

Fig. 6. Relative fraction of the KEDs corresponding to the high-energy contribution, $I_{HE}/(I_{LE} + I_{HE})$. See the text for detail.

ratio required for the peak decomposition. Nevertheless, the energy spectra of Fig. 7 suggest that the high-energy contribution is also important for the 2 keV measurement.

Between the singular, 2 keV, bombardment conditions and the other measurements, both the impact energy and angle have changed significantly. As Fig. 5 shows the insensitivity of the KEDs on the primary beam energy between 7 and 22 keV, we might speculate that the difference observed at 2 keV is rather related to the important variation of the primary beam angle. To check this hypothesis, simulations of the different bombardment conditions have been performed using TRIM calculations.

3.3 TRIM results

Although the TRIM code is obviously not suited to model the emission of molecular ions from polymers, we believe that it may provide a quite accurate determination of the primary ion ranges in the organic solid [39]. Parameters like the stopping powers, the number of displaced atoms and the energy of the recoils are well predicted by TRIM, too. In this study, TRIM was used to investigate the development of the

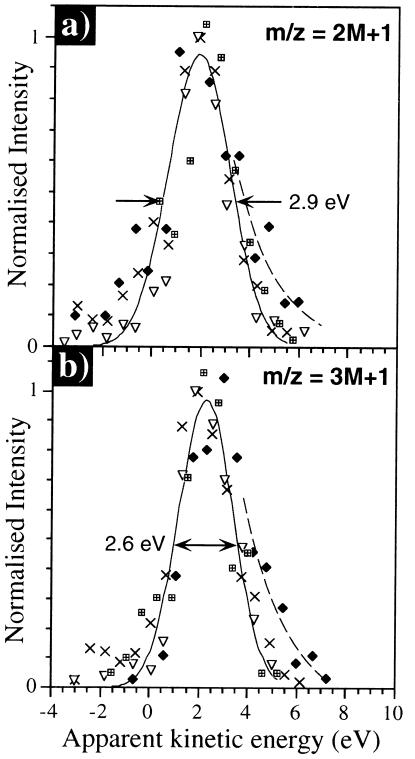

Fig. 7. Kinetic energy distributions of large molecular ions sputtered from PET samples bombarded 2–22 keV In^+ primary ions. (a) Dimer ion for 2 (closed circle), 7 (crosses), 12 (inverted open triangles), and 22 keV (plus sign inside squares) In^+ bombardment; (b) ibidem for the trimer ion.

collision cascades in the solid for the different bombardment conditions used in practice, under the assumption that these basic features of the energetic beam–solid interaction should not be strongly affected by the fine structure of the polymer (e.g. the one-dimensional character of the chains). An organic solid with the PET stoichiometric fractions of carbon, oxygen and hydrogen, as defined in the compound library of the software [40], served as target to simulate the 2, 7, 12, and 22 keV experimental conditions described in the previous sections (see Table 1). Keeping in mind the inherent limitations of TRIM, the interpretation of the results will be restricted to range and energy loss considerations and the sputtering yields, improperly modeled, will not be discussed.

To gain an insight into the size of the excited

Table 2
Ranges and energy loss of indium primary ions implanted in PET (TRIM)

Impact energy and angle (keV; deg)	Average range (Å)	Lateral range (Å)	Average nuclear energy loss[a] (eV/Å)	Average energy absorbed by carbon[a] (eV/Å)
2; 65	26	57	95	62
7; 43	87	85	109	64
12; 40	127	107	135	80
22; 38	189	147	140	90

[a] Average value calculated for the first 10 Å.

volume, the corresponding ranges are listed in Table 2. The size of the excited volume should be roughly proportional to the product of the vertical (projected on the *z* axis) and lateral ranges (projected on the *x*–*y* plane). As expected, the results indicate that this size increases proportionally to the primary beam energy. For the 7, 12, and 22 keV bombardment, the value of the vertical range is larger or equivalent to that of the lateral range. In contrast, the lateral range is more than two times greater than the vertical range for the 2 keV measurement. The extremely low penetration depth at 2 keV shows that the collision cascades are mostly confined in the first 25 Å below the polymer surface. Under these conditions, the backscattered ion yield calculated by TRIM is close to 0.1%, which is comparable to the measured In^+ secondary ion yields. The high yield of low-energy, backscattered ions explains the intense indium peak observed in Fig. 1(a).

On the other hand, the nuclear energy loss values in the top surface region (first 10 Å) increase by less than 50% between the 2 and 22 keV bombardment conditions (Table 1). In particular, the variation of the nuclear energy loss is less than 15% between 2 and 7 keV and the energy transferred to the carbon atoms of the PET is similar for this two cases, while the experimental SI yields increase by a factor of 2. Moreover, the increase of the nuclear stopping power reported in Table 2 between 7 and 22 keV corresponds to a decrease of the molecular ion intensities in the mass spectra. Although not shown in Table 2, the electronic energy loss follows a variation similar to the nuclear stopping power. Based on these calculations, a simple proportionality between the molecular ion yields and the nuclear or electronic stopping power is thus excluded in this range of experimental conditions.

The number of displaced atoms in the surface region is indicated by the average number of vacancies calculated by TRIM. The absolute values are shown in Fig. 8(a) (inset) for the first 50 Å below the

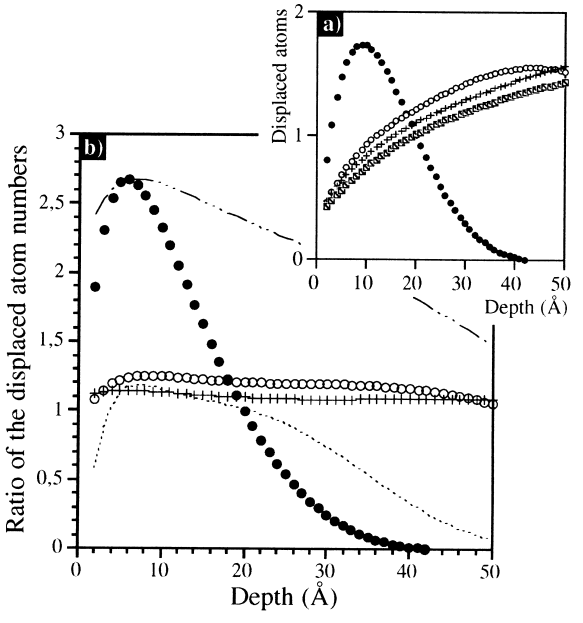

Fig. 8. TRIM simulation of the number of displaced atoms per primary ion (vacancies) in the surface region as a function of the primary In^+ beam bombardment conditions. (a) Absolute values for {2 keV; 65°} (closed circle), {7 keV; 43°} (open circle), {12 keV; 40°} (plus sign), and {22 keV; 38°} (slashed square); (b) values normalised by that obtained for the {22 keV; 38°} bombardment conditions. The dashed lines correspond to virtual bombardment conditions described in the text: {2 keV; 40°} (ellipse) and {12 keV; 65°} (dashed ellipse).

surface. (Note that, experimentally, these 50 Å correspond to the upper limit of the atomic ion emission depth for polymeric coatings [45].) The difference between the 2 keV bombardment and the other experimental conditions is striking. Although the number of vacancies created in the solid increases slowly to a maximum located around 40–50 Å (7 keV bombardment) or deeper for the higher energy conditions, the vacancy distribution at 2 keV peaks around 10 Å and decreases to 10% of its maximum value after 30 Å. For comparison purpose, the vacancy distribution at 2, 7, and 12 keV have been divided by the distribution obtained at 22 keV [Fig. 8(b)]. In the first 50 Å, the ratio is constant and close to one for 7 and 12 keV. Thus, in the surface region, the deposited energy (see Table 2), but also the number of displacements do not vary drastically between 7 and 22 keV. In contrast, the shape of the curve is completely different at 2 keV: the average number of vacancies is much larger in the first 20 Å (2.5 times greater at 10 Å) and it decreases quickly beyond that depth.

To check whether the angle or the energy is the dominant parameter to explain the observed ratios in the extreme surface region, other In^+ beam conditions have been simulated, i.e. {2 keV; 40°} and {12 keV; 65°}. They are indicated by dashed lines in Fig. 8(b). For the {2 keV; 40°} conditions, the ratio is close to 1 between 5 and 20 Å and decreases softly beyond 20 Å. The maximum "plateau" value is thus very close to that calculated for the 7 and 12 keV bombardment conditions used in practice. In contrast, the ratio is close to 2.5 between 0 and 20 Å for the {12 keV; 65°} conditions, which is similar to the experimental 2 keV bombardment conditions. These complementary calculations indicate that the effect of the impact angle is predominant to explain the number of displacements in the extreme surface region.

Interestingly, TRIM also calculates the number of internuclear energy transfers that do not generate vacancies, because the involved energy is lower than the binding energy in the solid (a few electron volts). The shape of the distributions of these "vibrational" energy transfers is very similar to that of vacancies but their absolute number is more than one order of magnitude greater (Fig. 9). Again, the number of these excitations produced in the topmost surface layer is mainly influenced by the impact angle, rather than by the impact energy.

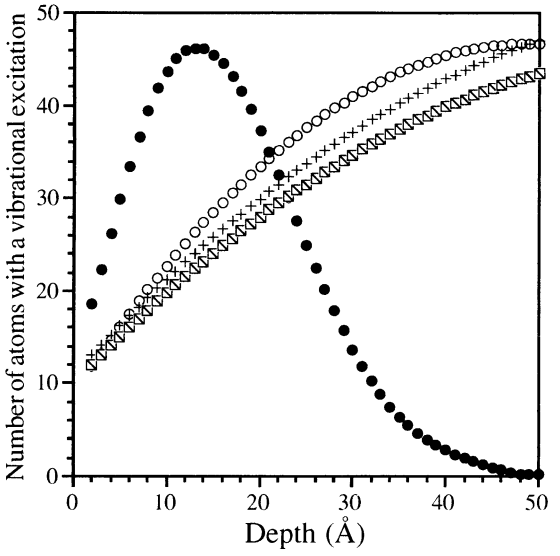

Fig. 9. TRIM simulation of the number of vibrationally excited atoms (phonons) in the surface region as a function of the primary In^+ beam bombardment conditions. Absolute values for {2 keV; 65°} (closed circle), {7 keV; 43°} (open circle), {12 keV; 40°} (plus sign), and {22 keV; 38°} (slashed square).

4. Discussion

The influence of the primary beam energy on the molecular ion yields will be discussed in detail in [11]. Nevertheless, for 7–22 keV indium bombardment, our results show unambiguously that the measured yields are not proportional to the nuclear or electronic stopping powers. On the other hand, the yield increase observed between 2 and 7 keV is consistent with the literature *if the influence of the energy predominates over the effect of the impact angle*. Indeed, the yield increase reported in the literature when changing from 40° to 65° incidence angle [29,30] is not observed in our measurements.

The comparison between Ga^+ and In^+ (Cs^+) primary beams shows that the effect of the ion beam nature on the fragmentation of PET is dramatic. The influence of the primary beam energy on this param-

eter is weaker. However, the regular increase of fragmentation observed between 2 and 22 keV for In^+ bombardment suggests again that the influence of the energy on the relative yields is greater than that of the impact angle in the considered range of experimental conditions.

If one excludes the 2 keV data, the observed independence of the KEDs on the primary ion nature and energy indicates that the kinetic energy of molecular ions is governed by the energy required for the particular fragmentation channel leading to their production, rather than by the primary beam characteristics. It is consistent with our previous interpretations connecting the kinetic and internal energies of molecular ions to the degree of fragmentation with respect to the precursor, in the context of collisional sputtering [9]. This insensitivity can be understood assuming that the molecular ion emission processes, constituting the late stages of the ion–solid interaction, are almost completely independent on the early primary ion scattering events where the energy transfer from the primary ion to the matrix occurs. In this respect, the increase of the ejection time with increasing particle size has been demonstrated by MD simulations for organic [46] and inorganic clusters [47,48].

The stopping powers as well as the amount of displacements and vibrational excitations calculated by TRIM for 7, 12, and 22 keV ion bombardment indicate that several of the relevant parameters in the sputtering process vary weakly in this range of experimental conditions. Although a direct comparison is impossible, these simulations are not in contradiction with the identical KEDs measured by TOF SIMS in the same conditions. In this context, the yield variation would be explained, for instance, by a difference in the size of the excited area at the surface, rather than by different emission mechanisms. Instead, the 2 keV KED measurement and the corresponding simulation show both very peculiar features. The important number of backscattered ions in the positive SIMS spectrum is qualitatively predicted by TRIM. In addition, the increased number of displaced atoms and vibrational excitations together with the concentration of the collision cascades in the extreme surface region might explain different emission processes for molecular ions. For example, we can speculate that the probability of ejection due to a co-operative motion of the target atoms, or to the collective vibration of several nuclei might be increased in these conditions. In addition, the correlated momentum transfer due to collective motion of several target atoms could explain the high kinetic energy contribution observed in the energy spectra of molecular ions sputtered under 2 keV ion bombardment [6]. These hypotheses should be verified using more sophisticated simulation algorithms (molecular dynamics [35,46]).

5. Conclusion

Several new results concerning the sputtering of molecular ions from PET surfaces have been brought to light by the use different primary ion bombardment conditions (nature, energy and angle). (1) For indium primary ions (1.67×10^8 ions per spectrum), the molecular ion yields increase between 2 and 7 keV, undergo a maximum at 7 keV and decrease up to 22 keV; (2) the fragmentation of PET into low-mass molecular ions increases with decreasing primary ion mass (Ga^+ in comparison to In^+, Cs^+) and, unexpectedly, with increasing primary ion energy ($2 \leq E \leq 22$ keV); (3) for the {2 keV; 65°} bombardment, the yield of backscattered indium is comparable to that of sputtered PET ions. This behaviour, as well as the predominance of low-energy backscattered ions (below 10 eV), is qualitatively predicted by TRIM; (4) the KED of Na^+ becomes narrower with decreasing primary beam energy, as reported in the literature for atomic ions; (5) the KED of molecular ions sputtered from PET is almost independent of the primary ion nature and energy, except for the 2 keV measurement. In this case, the fraction of molecular ions with a "high" kinetic energy (5–6 eV) is significantly greater and it increases with the ion size. TRIM calculations suggest that this might be related to the increase of the incidence angle accompanying the reduction of the beam energy in our system. In the {2 keV; 65°} bombardment conditions, the concentration of the cascades in the surface region (25 Å), as well as the augmentation of the atomic displacement and vibra-

tional excitation numbers by a factor of 2 or more, lead us to propose that a larger number of "high energy" ions might be sputtered by collective mechanisms. To improve the interpretation of the results, more complex MD simulations are required.

Acknowledgements

The authors wish to thank C. Poleunis for his collaboration to the experimental part of this study and S. Netcheva for her help and advice concerning the TRIM calculations. This work is supported by the "Action de Recherche Concertée" (94/99-173) of the "Communauté Française de Belgique" and by the Belgian Interuniversity Attraction Pole Program (PAI-IUAP P4/10) on "Reduced Dimensionality systems." The TOF SIMS equipment was acquired with the support of the "Région Wallonne" and "FRFC-Loterie Nationale" of Belgium.

References

[1] P. Bertrand, L.T. Weng, in Surface Characterization, A User's Sourcebook, D. Brune, R. Hellborg, H.J. Whitlow, O. Hunderi (Eds.), Wiley, New York, 1997, p. 344.
[2] The Wiley Static SIMS Library, Wiley, New York, 1996.
[3] A. Delcorte, P. Bertrand, Nucl. Instrum. Methods B 115 (1996) 246.
[4] A. Delcorte, P. Bertrand, SIMS X Proceedings, A. Benninghoven, B. Hagenhoff, H.W. Werner (Eds.), Wiley, New York, 1997, p. 731.
[5] A. Delcorte, P. Bertrand, Nucl. Instrum. Methods B 135 (1998) 430.
[6] A. Delcorte, P. Bertrand, Surf. Sci. 412/413 (1998) 97.
[7] A. Delcorte, B.G. Segda, P. Bertrand, Surf. Sci. 381 (1997) 18; 389 (1997) 393.
[8] A. Delcorte, P. Bertrand, SIMS XI Proceedings, R. Lareau, G. Gillen (Eds.), Wiley, New York, 1998, p. 447.
[9] A. Delcorte, P. Bertrand, Nucl. Instrum. Methods B 117 (1996) 235.
[10] A. Delcorte, P. Bertrand, Int. J. Mass Spec., 184 (1999) 217.
[11] D.F. Reich, X. Vanden Eynde, C. Poleunis, A. Delcorte, P. Bertrand, unpublished.
[12] D.F. Reich, presented at the 11th SIMS Workshop, Austin, 10–13 May, 1998.
[13] H.H. Andersen, H.L. Bay, in Sputtering by Particle Bombardment I, R. Behrisch (Ed.), Springer Verlag, Berlin, 1981, p. 145.
[14] A. Benninghoven, F.G. Rüdenauer, H.W. Werner, Secondary Ion Mass Spectrometry, Wiley, New York, 1987, p. 699.
[15] P. Sigmund, in Sputtering by Particle Bombardment I, R. Behrisch (Ed.), Springer Verlag, Berlin, 1981, p. 9.
[16] H.L. Bay, Nucl. Instrum. Methods B 18 (1987) 430.
[17] R.G. Hart, C.B. Cooper, Surf. Sci. 94 (1980) 105.
[18] K. Wittmaack, Surf. Sci. 90 (1979) 557.
[19] M. Urbassek, Nucl. Instrum. Methods B 4 (1984) 356.
[20] W. Eckstein, Computer Simulation of Ion Solid Interactions, U. Gonser, A. Mooradian, R.M. Osgood, M.B. Panish, H. Sakaki (Eds.), Springer Verlag, Berlin, 1991.
[21] W. Eckstein, Nucl. Instrum. Methods B 18 (1987) 344.
[22] W. Ens, Mat. Fys. Medd. Dan Vid Selsk. 43 (1993) 155.
[23] A. Benninghoven, in Ion Formation from Organic Solids, Springer Series in Chemical Physics Vol. 25, A. Benninghoven (Ed.), Springer-Verlag, Berlin, 1983, p. 64.
[24] D. Briggs, M.J. Hearn, Int. J. Mass Spectrom. Ion Processes 67 (1985) 47.
[25] B.E. Winger, O.W. Hand, R.G. Cooks, Int. J. Mass Spectrom. Ion Processes 84 (1988) 89.
[26] R. Galéra, J.C. Blais, G. Bolbach, Int. J. Mass Spectrom. Ion Processes 107 (1991) 531.
[27] G. Bolbach, R. Beavis, S. Della-Negra, C. Deprun, W. Ens, Y. Lebeyec, D.E. Main, B. Schueler, K.G. Standing, Nucl. Instrum. Methods Phys. Res. B 30 (1988) 74.
[28] R. Galéra, G. Bolbach, O. Bouloussa, J.C. Blais, in Secondary Ion Mass Spectrometry, SIMS VIII Proceedings, A. Benninghoven, K.T.F. Janssen, J. Tümpner, H.W. Werner (Eds.), Wiley, New York, 1992, p. 21.
[29] S.A. Martin, C.E. Costello, K. Biemann, Anal. Chem. 54 (1982) 2362.
[30] W. Szymczak, K. Wittmaack, J. Phys. C 2 (1989) 75.
[31] T. Hoshi, S. Yamada, S. Yoshida, T. Watanabe, M. Kudo, in Secondary Ion Mass Spectrometry, SIMS X Proceedings, A. Benninghoven, B. Hagenhoff, H.W. Werner (Eds.), Wiley, New York, 1997, p. 255.
[32] T. Hoshi, S. Yoshida, T. Watanabe, Y. Ichinohe, K. Endo, Z. Liu, M. Kudo, in Secondary Ion Mass Spectrometry, SIMS XI Proceedings, G. Gillen, R. Lareau, J. Bennett, F. Stevie (Eds.), Wiley, New York, 1998, p. 475.
[33] T. Hoshi, M. Tozu, R. Oiwa, L. Zhanping, M. Kudo, Appl. Surf. Sci. 121/122 (1997) 146.
[34] B.J. Garrison, J. Am. Chem. Soc. 104 (1982) 6211.
[35] R. Zaric, B. Pearson, K.D. Krantzman, B.J. Garrison, Int. J. Mass Spectrom. Ion Processes 174 (1998) 155.
[36] R.S. Taylor, C.L. Brummel, N. Winograd, B.J. Garrison, J.C. Vickerman, Chem. Phys. Lett. 233 (1995) 575.
[37] B.W. Schueler, Microsc. Microanal. Microstruct. 3 (1992) 119.
[38] A. Delcorte, L.T. Weng, P. Bertrand, Nucl. Instrum. Methods B 100 (1995) 213.
[39] J.P. Biersack, in Ion Beam Modification of Insulators, P. Mazzoldi, G.W. Arnold (Eds.), Elsevier, Amsterdam, 1987, p. 26.
[40] Information concerning this program can be found at the following internet address: http://www.research.ibm.com/ionbeams/SRIM/
[41] F.-R. Lang, Y. Pitton, H.J. Mathieu, D. Landolt, E.M. Moser, Fres. J. Anal. Chem. 358 (1997) 251.
[42] A. Delcorte, P. Bertrand, E. Wischerhoff, A. Laschewsky, Langmuir 13 (1997) 5125.
[43] L. Kelner, S.P. Markey, Int. J. Mass Spectrom. Ion Processes 59 (1984) 157.

[44] G. Gillen, Int. J. Mass Spectrom. Ion Processes 105 (1991) 215.
[45] A. Delcorte, P. Bertrand, X. Arys, A. Jonas, E. Wischerhoff, B. Mayer, A. Laschewsky, Surf. Sci. 366 (1996) 149.
[46] K. Beardmore, R. Smith, Nucl. Instrum. Methods B 102 (1995) 223.
[47] G. Betz, W. Husinsky, Nucl. Instrum. Methods B 102 (1995) 281.
[48] Th. J. Colla, H.M. Urbassek, A. Wucher, C. Staudt, R. Heinrich, B.J. Garrison, C. Dandachi, G. Betz, Nucl. Instrum. Methods B 143 (1998) 284.